Supporting Information for:

Chemical Properties and Single Particle Mixing State of Soot Aerosol in Houston during the TRACER Campaign

Ryan N. Farley[1,2], James E. Lee[3], Laura-Hélèna Rivellini[4], Alex K. Y. Lee[5], Rachael Dal Porto[6], Christopher D. Cappa[2,6], Kyle Gorkowski[3], Abu Sayeed Md Shawon[3], Katherine B. Benedict[3], Allison C. Aiken[3], Manvendra K. Dubey[3], Qi Zhang[1,2]

[1]Department of Environmental Toxicology, University of California Davis, CA, 95616, USA

[2]Agricultural and Environmental Chemistry Graduate Group, University of California Davis, CA, 95616, USA

[3]Earth and Environmental Sciences Division, Los Alamos National Laboratory, Los Alamos, NM, USA

[4] Department of Chemistry, University of Toronto, Toronto, ON, Canada

[5]Air Quality Processes Research Section, Environment and Climate Change Canada, Toronto, ON, Canada

[6]Department of Civil and Environmental Engineering, University of California, Davis, CA, 95616 USA

Correspondence to: Qi Zhang (dkwzhang@ucdavis.edu)

1. Methods

S1.1 Co-located Measurements at La Porte Field Site

Measurements of numerous aerosol chemical and physical properties were collected at the La Porte site during the TRACER campaign. Ambient aerosols were sampled from a mast approximately ten meters above ground level prior to passing through a nafion drier followed by a $PM_{2.5}$ cyclone (Fig. S1) . The flow was then split between all instrumentation within the trailer. In addition to the laser-only SP-AMS, a second, co-located SP-AMS with a $PM_{2.5}$ inlet was operated in the dual vaporizer mode to simultaneously measure non-refractory $PM_{2.5}$ (NR-$PM_{2.5}$) and rBC. The dual vaporizer SP-AMS utilizes both a laser vaporizer and a resistively heated tungsten thermal vaporizer (600°C) to convert particles into the gas phase for ionization (Avery et al., 2020). The dual vaporizer SP-AMS was programmed to cycle between "laser-on" mode and "laser off" mode. During laser-off mode it functions equivalently to a conventional high-resolution time-of-flight aerosol mass spectrometer (HR-AMS) and only material that vaporizes at 600°C, including most organics and the ammonium salts of nitrate, sulfate and chloride, is measured. (DeCarlo et al., 2006; Onasch et al., 2012).

The BC number and mass concentrations were measured with a single particle soot photometer (SP2). Dry (<50% RH) and humidified (85% RH) aerosol absorption, scattering, and extinction were measured at 405 and 532 nm using a two-wavelength cavity ringdown-photoacoustic spectrometer (CRD-PAS) (Langridge et al., 2011).

Meteorological data, including temperature, relative humidity, precipitation rate and wind speed, were measured on site. Ozone concentration was measured using an Ozone Analyzer (Thermo-Fisher Scientific). Trace gas measurements were performed at the Texas Commission of Environmental Quality (TCEQ) Deer Park site, located 6 km from the La Porte sampling location (Figure S1). Hourly NO, NO_2 and SO_2 concentrations were retrieved from the TCEQ website (https://www.tceq.texas.gov/cgi-bin/compliance/monops/daily_summary.pl?cams=35, last access 8/25/2023).

S1.2 Soot-Particle Aerosol Mass Spectrometer Operation

The laser-only SP-AMS was programmed to automatically switch between mass spectrum (MS) only mode, combined MS/ePToF mode, and event trigger single particle (ETSP) mode. Each mode lasted 5 minutes, with two runs of MS/ePToF resulting in a total cycle time of 20 minutes. The *m/z* range for MS/ePToF and ETSP was 10 - 317 amu, however for the MS-only runs, the *m/z* range was increased to 900 amu to investigate the presence of fullerene soot clusters.

Calibration of the SP-AMS ionization efficiency (IE) was performed using dried monodisperse ammonium nitrate (NH_4NO_3) aerosol (Canagaratna et al., 2007; Jayne et al., 2000). The relative ionization efficiencies (RIE) of ammonium, sulfate and chloride were determined using ammonium nitrate, ammonium sulfate and ammonium chloride respectively, and found to be 3.14, 1.15 and 1.43. The RIE for nitrate was corrected for ions other than NO^+ and NO_2^+ and was found to be 1.05. Particle size calibration was conducted using polystyrene latex spheres (PSLs) ranging from 97 nm to 800 nm prior to and following deployment. Because vaporization of pure ammonium salts and PSLs requires the tungsten vaporizer, the above-mentioned calibrations were performed both before and after the instrument deployment. The RIE of rBC was determined using size

selected regal black (Cabot Corp) following the removal of the thermal vaporizer. Two independent calibrations were performed prior to the start of sampling and following the end of sampling, and an RIE of 0.28 was determined for rBC.

The organic CO_2^+ signal was corrected for the influence from $CO_{2(g)}$ by subtracting the time dependent gas-phase measurements from a collocated AERIS CO_2 monitor. The ammonium signal was constrained to the NH_2^+ peak, as the NH_3^+ had an elevated background due to interference from the OH^+ peak and NH^+ was influenced by the $^{15}N^+$ peak. The ratio of NH^+/NH_2^+ (0.07) and NH_3^+/NH_2^+ (1.18) measured during the ammonium nitrate calibration were used.

A coating thickness dependent collection efficiency (CE) was applied as was done previously (Collier et al., 2018; Willis et al., 2014). The following sigmoidal relation from Collier et al. (2018) was used:

$$E = 0.34 + \left[\frac{0.16}{1+\exp\left(\frac{2.5-\frac{R_{coat}}{BC}}{0.19}\right)}\right] \quad \text{(S1)}$$

Where $R_{coat/BC}$ is the mass ratio of coating material to rBC. As can be seen from this equation, the CE ranged from 0.34 for the most thinly coated particles, to 0.5 for more thickly coated particles. This correction is needed because thickly coated particles produce a narrower particle beam, resulting in better particle beam – laser beam overlap.

S1.3 Positive Matrix Factorization Analysis

Positive Matrix Factorization (PMF) was conducted with both organic and inorganic ions included in the mass spectral matrix. The inorganic ions used were $C_{1\text{-}4}^+$ for rBC, SO^+, SO_2^+, HSO_2^+, SO_3^+, HSO_3^+, $H_2SO_4^+$ for sulfate, NO^+ and NO_2^+ for nitrate, and K^+. Ammonium ions were not included due to uncertainty from interference with water signal and chloride was not included due to low signal to noise. The matrix was prepared using previously established guidelines (Ulbrich et al., 2009; Zhang et al., 2011). Noisy ions with S/N < 0.2 were removed while ions with S/N < 2 and those scaled to CO_2^+ (i.e., O^+, OH^+, H_2O^+, CO^+) were downweighted.

The four-factor solution was chosen as the best solution based on analysis of the temporal and spectral features. Progressing from three factors to four factors resulted in the separation of a factor dominated by potassium and a decrease in the total residual. However, the five-factor solution shows non-meaningful splitting of the sulfate factor. The rotational ambiguity was explored by varying the fPeak between -1 and 1, however these solutions showed negligible change in Q/Q_{exp} and splitting of the sulfate factor therefore an fpeak equal to zero was selected.

S1.4 Estimating Organic Elemental Ratios from ETSP results

The average atomic oxygen/carbon (O/C) and hydrogen/carbon (H/C) ratios for single particle spectra were estimated by linear decomposition. The improved ambient (IA) ratios were first calculated for the ensemble measurements using the high resolution mass spectra (Canagaratna et al., 2015). The elemental ratios were decomposed to the organic fraction at *m/z* 43

(f_{43}), 44 (f_{44}), 55 (f_{55}) and 57 (f_{57}). Time points with OA concentrations < 0.5 μg m^{-3} were removed to avoid noisy data points. The results of decomposition are as follows:

$$O/C = (1.899 * f_{43}) + (3.968 * f_{44}) + (4.173 * f_{55}) + (2.178 * f_{57}) \quad (S2)$$

$$H/C = (7.571 * f_{43}) + (2.078 * f_{44}) + (14.39 * f_{55}) + (8.602 * f_{57}) \quad (S3)$$

These equations were then used to reconstruct the elemental ratios for each single particle spectra. The reconstructed values capture the variation in O/C well (slope = 0.97, r^2 = 0.74) but show more scatter for H/C (slope = 1.0, r^2 = 0.21). The variation of these ratios for each particle class is shown in figure S11.

S1.5 Predicting Single Particle Aerosol Hygroscopicity

Hygroscopicity of single particles was predicted using Zdanovskii-Stokes-Robinson (ZSR) mixing rule and the hygroscopicity paramter (κ) introduced in Petters and Kreidenweis (2007). This method assumes that the overall hygroscopicity of an aerosol is proportional to the κ value of each component, weighted by the respective volume faction. For any particle *i*, κ_i can be calculated as:

$$\kappa_i = \sum_1^j \kappa_j V_{i,j} \quad (S4)$$

Where κ_j is the hygroscopicity parameter for pure compound *j*, and $V_{i,j}$ is the volume fraction of compound j in particle *i*. The density and κ for all compounds used are shown in table S2. The volume fraction for individual particles was calculated by dividing the measured mass concentration for particle events measured by ETSP mode by the assumed density of each species. Nitrate and chloride were assumed to be in the form of their ammonium salts. Sulfate was first apportioned to potassium sulfate using the measured K^+ signal, and all remaining sulfate was assumed to be in the form of ammonium sulfate. The organic density was parameterized based on the method described in Kuwata et al. (2012).

$$\rho = 12 + (H/C) + 16 * (O/C) / [7 + 5 * (H/C) + 4.15 * (O/C)] \quad (S5)$$

The organic hygroscopicity was estimated from the paramaterization introduced in Duplissy et al. (2011).

$$\kappa = 2.2 * f_{44} - 0.13 \quad (S6)$$

The choice of species has important implications on the results, as this will alter both the volume fraction and the hygroscopicity and a brief explanation of the assumptions is given here. In addition to ammonium salts, atmospheric anions can also be found as sodium salts (i.e. $NaNO_3$, NaCl, Na_2SO_4). However, low concentrations of Na^+ was measured by the SP-AMS and these compounds were assumed to be negligible. Atmospheric potassium can be found in a variety of forms. In addition to K_2SO_4, this commonly includes KNO_3 and KCl (Cao et al., 2019; Pratt et al., 2011; Zauscher et al., 2013). However, during periods of elevated K^+, there was a molar excess K^+ relative to NO_3^- or Cl^- suggesting that these were not the major species present. As mentioned above, ammonium was not included in the ETSP processing, therefore it was not possible to estimate the aerosol acidity or separate sulfate signal between $(NH_4)_2SO_4$, NH_4HSO_4 and H_2SO_4. Here, we make the assumption that the aerosol is neutralized and all sulfate not attributed to K_2SO_4 is in the form of ammonium sulfate.

The critical supersaturation value for individual particles was estimated by solving the following equation for S_c:

$$\kappa = \frac{4A^3}{27D_d^3 \ln^2 S_c} \quad \text{(S7)}$$

$$A = \frac{4\sigma_{s/a} M_w}{RT\rho_w} \quad \text{(S8)}$$

Where D_d is the dry aerosol diameter measured by SP-AMS, $\sigma_{s/a}$ is the surface tension of the solution/air interface, ρ_w is the density of water, M_w is the molecular weight of water, R is the universal gas constant and T is temperature. Here we assume values of $\sigma_{s/a}$ = 0.072 J m^{-2} and T = 298.15K (Petters and Kreidenweis, 2007).

S1.6 Back Trajectory Analysis

Backtrajectories were calculated using the Hybrid Single Particle Integrated Trajectory (HYSPLIT) model (Draxler and Hess, 1998). 240 hour back trajectories were initiated every 3 hours using the 1 degree Global Data Assimilation System (GDAS) meterology. Each trajectory was initiated at the sampling location at a height of 100 m above ground level. Concentration Weighted Trajectories (CWT) were calculated in the ZeFir program within Igor Pro to investiate potential geographical source regions (Petit et al., 2017).

S2. Figures

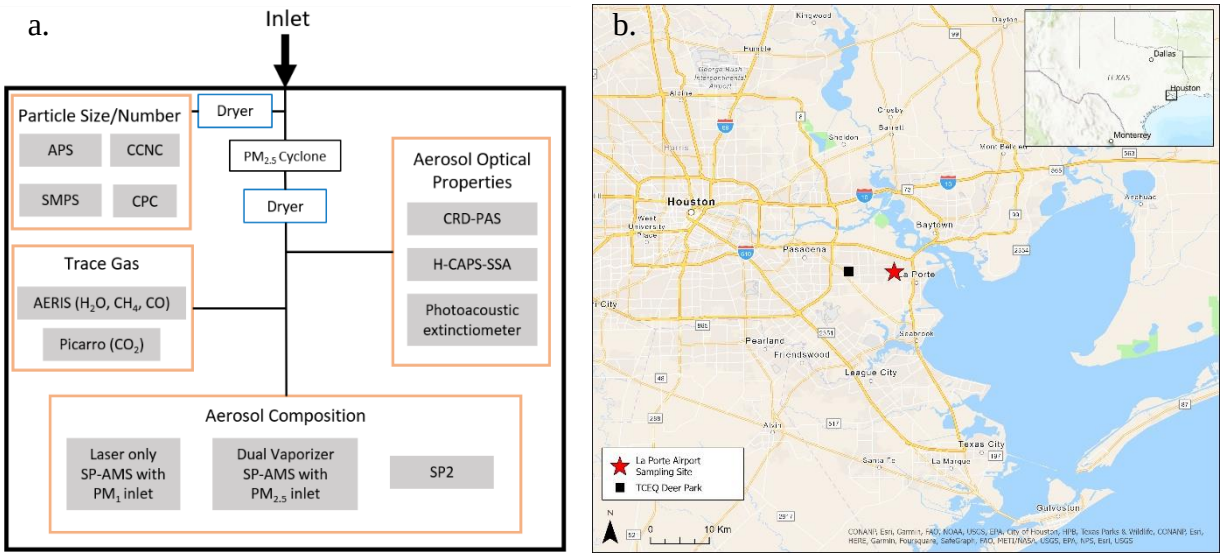

Figure S1: (a) Schematic of the experimental layout during the TRACER field campaign. Acronyms: APS: Aerodynamic Particle Sizer, CCNC: Cloud Condensation Nuclei Counter, SMPS: Scanning Mobility Particle Sizer, CPC: Condensation Particle Counter, CRD-PAS: Cavity Ring Down- Photoacoustic Spectrometer, H-CAPS-SSA: Humidified cavity-attenuated phase shift-single scattering albedo monitor, SP2: Single Particle Soot Photometer. (b) Map depicting the location of the La Porte sampling site (red star) in the greater Houston region.

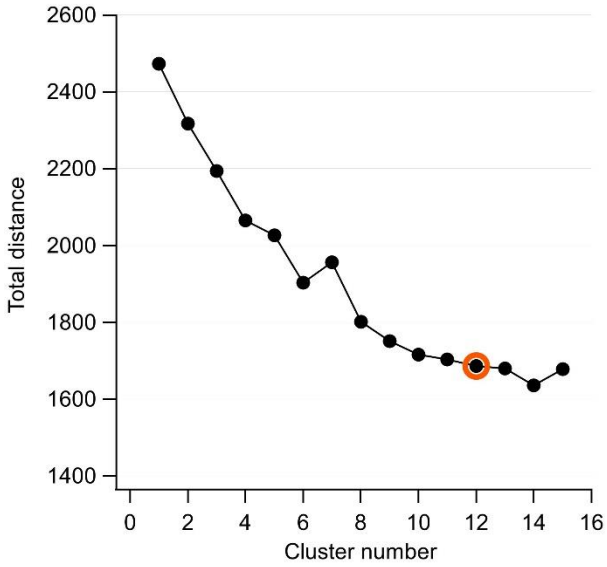

Figure S1: Total Euclidian distance between individual particles and the cluster average as a function of cluster number. The final 12-cluster solution is marked with the orange circle.

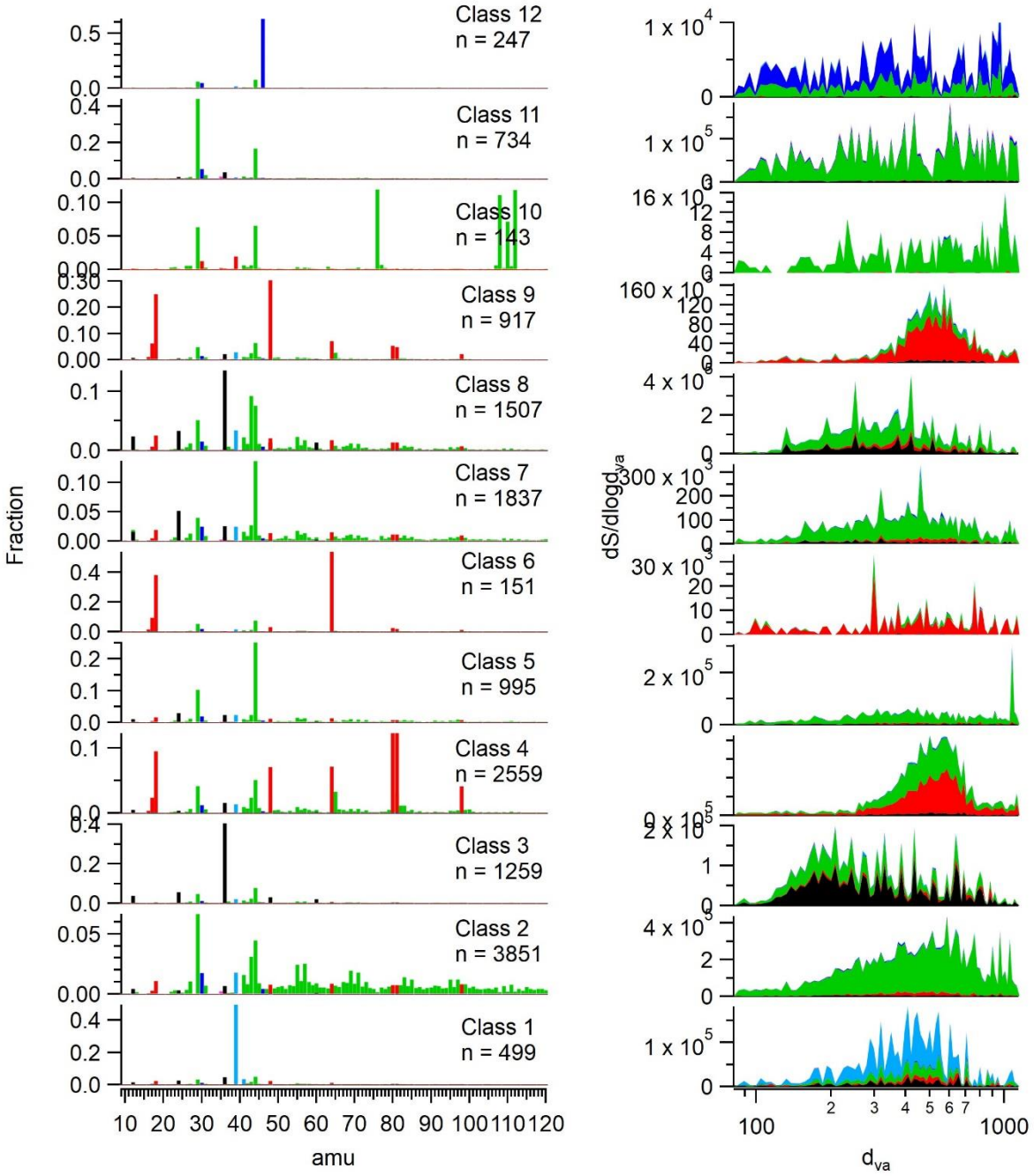

Figure S2: Average mass spectra and size distributions of particle clusters prior to merging similar clusters. Clusters 4, 6 and 9 were merged into a single sulfate cluster. Clusters 5 and 7 were merged into a single OOA cluster. Class 10 was discarded as a noise artifact.

145

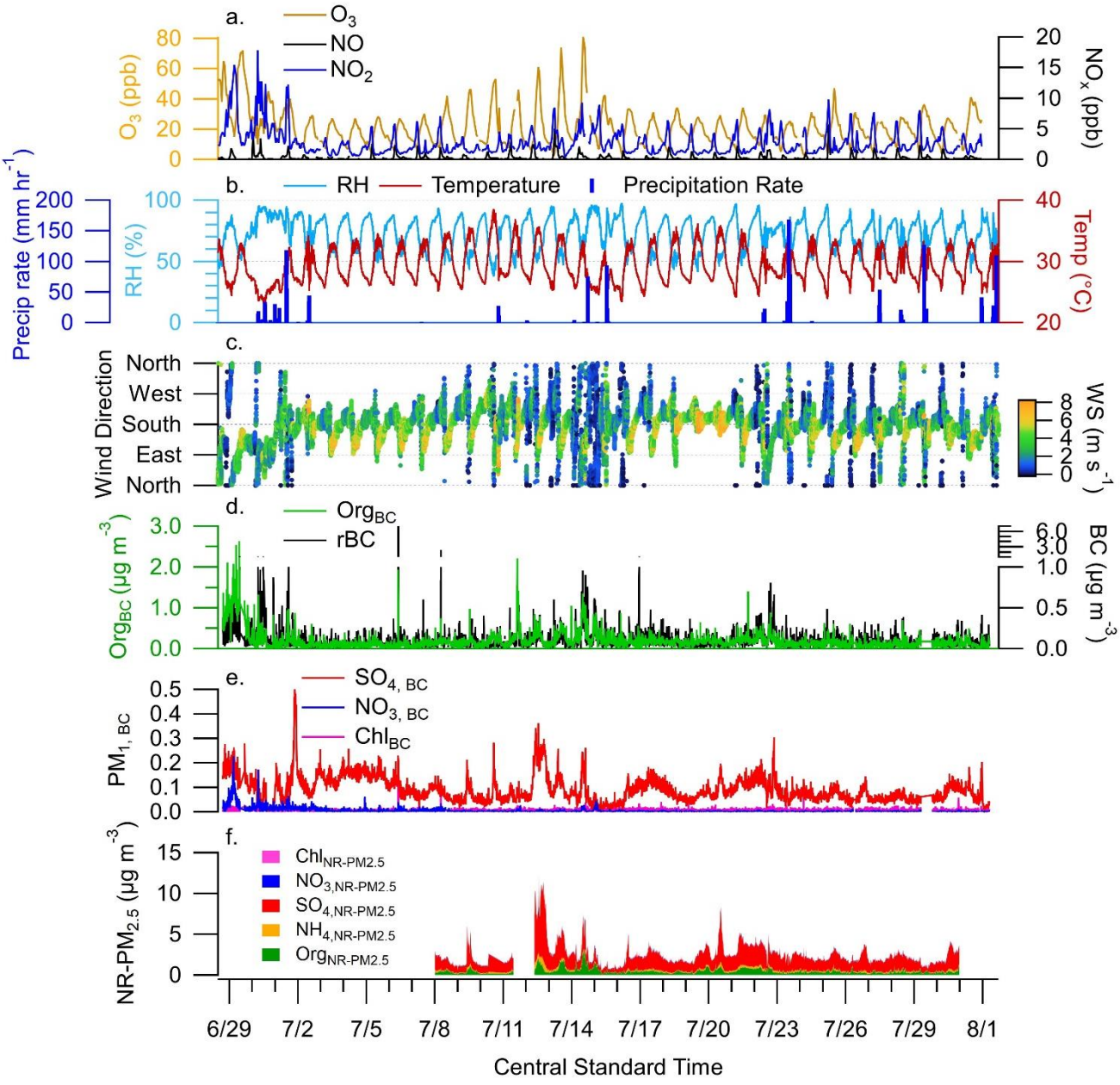

Figure S4: Time series of (a) trace gases, (b) meterological parameters, (c) wind speed and direction (d,e) rBC and associated coating material, (f) NR-$PM_{2.5}$ measured by co-located dual vaporizer SP-AMS in laser-off mode.

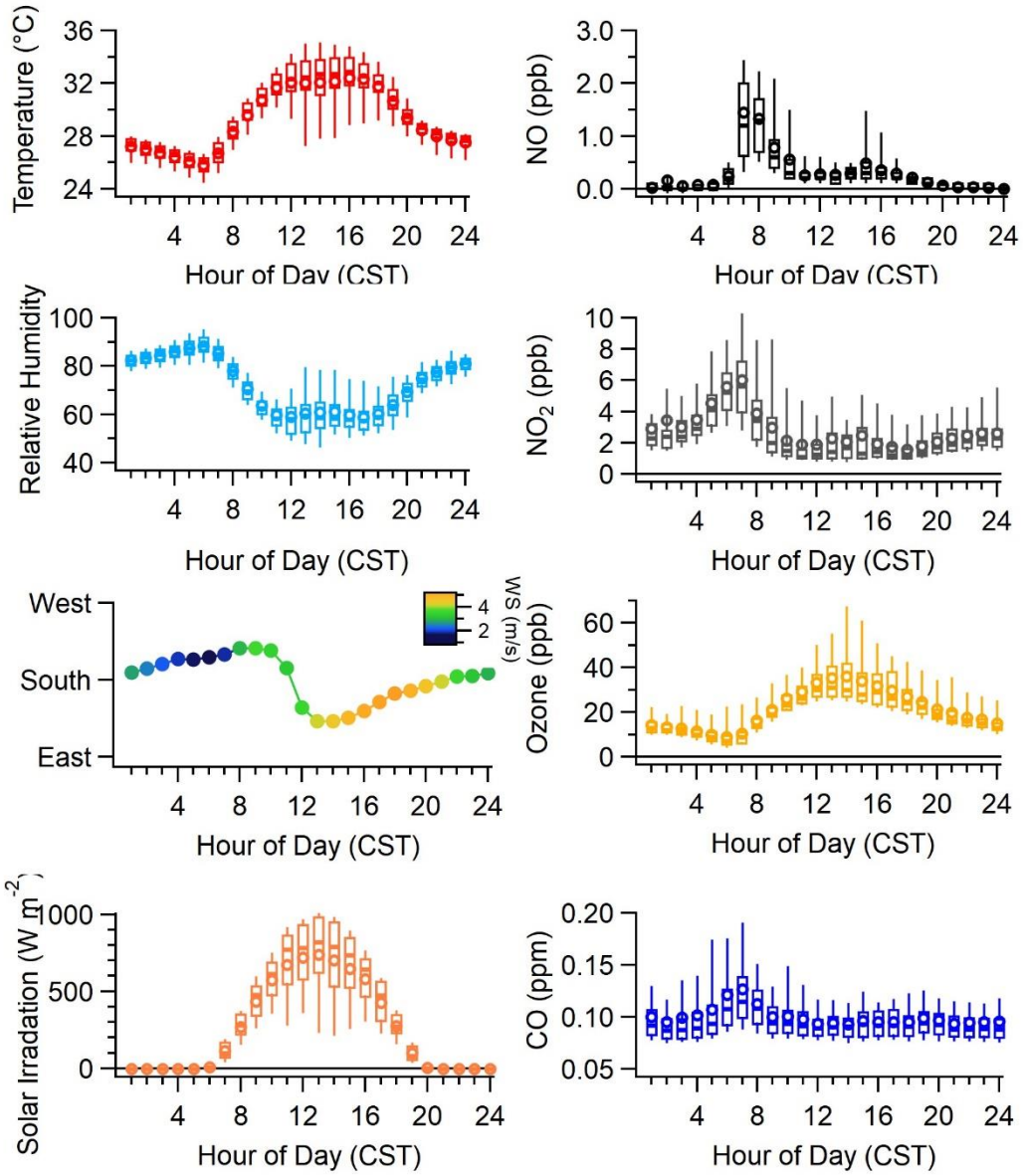

150

Figure S5: Diurnal variation in meteorological parameters and trace gas species. Solid and open symbols represent the median and mean respectively. Boxes indicate 25-75th percentile and whiskers indicate 10-90th percentiles.

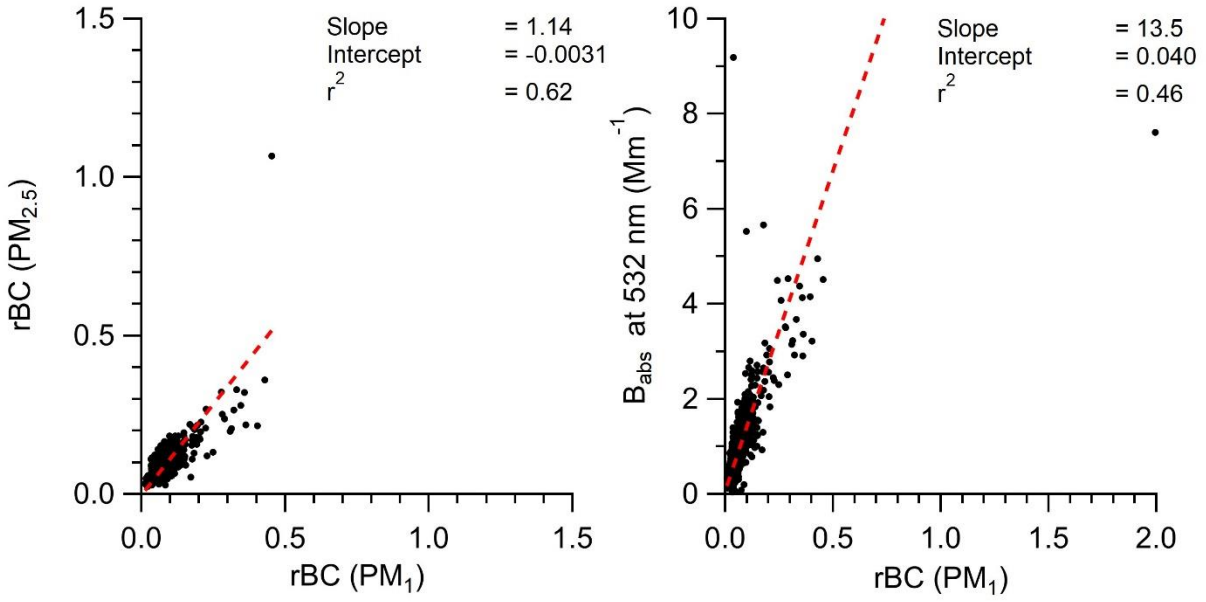

155 **Figure S6: (a) Correlation between rBC measured by dual vaporizer SP-AMS equipped with $PM_{2.5}$ lens and laser-only SP-AMS. (b) Correlation between aerosol absorption at 532nm measured by photoacoustic spectroscopy and rBC measured by laser-only SP-AMS. Fit lines are orthogonal distance regressions.**

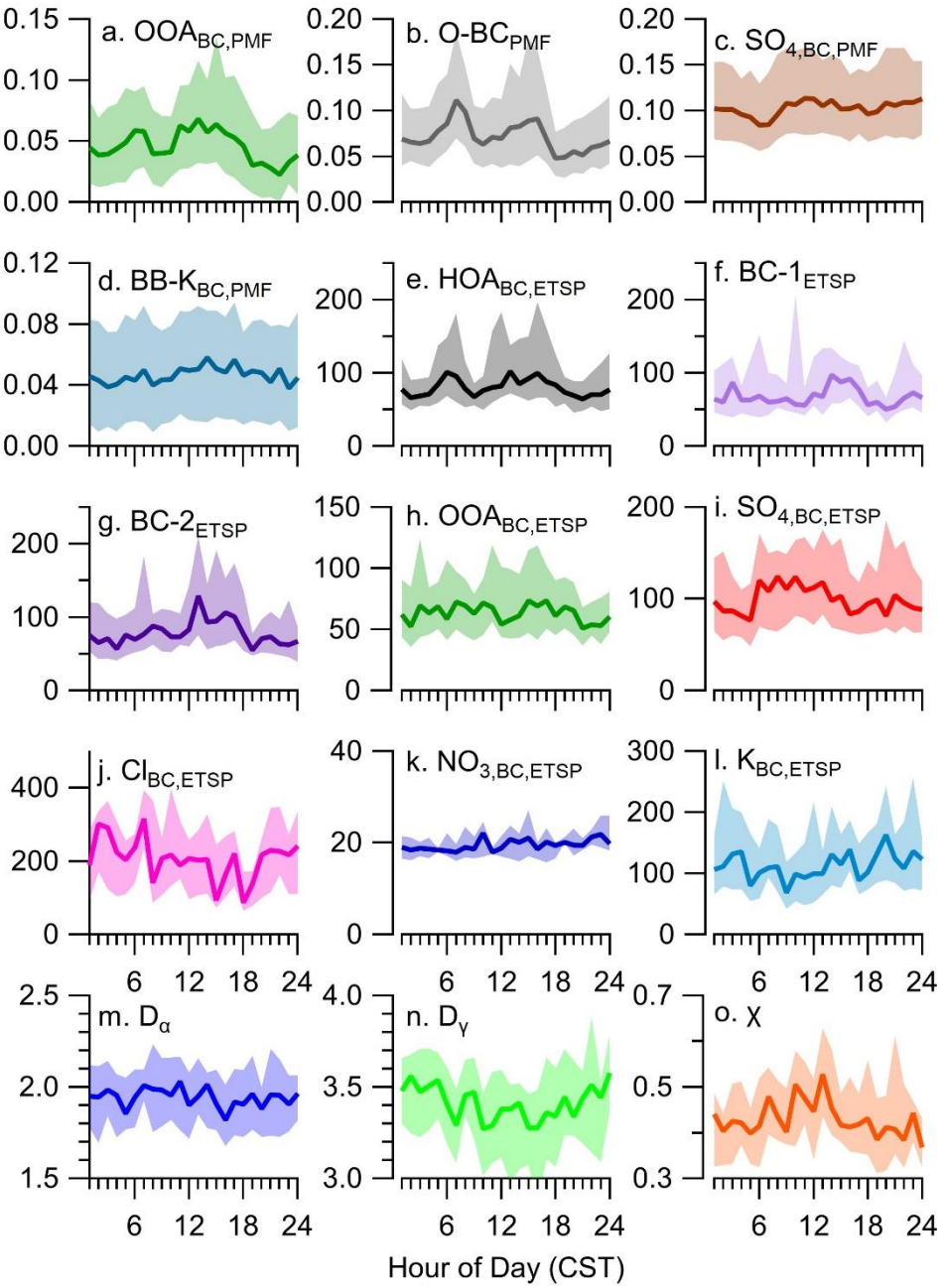

Figure S7: diurnal profiles of (a-d) PMF factors, (e-l) ETSP particle clusters, (m-o) mixing state metrics. Solid line is hourly median value and shaded area represents the interquartile range. Units for a-d are μg m^{-3} and e-l are ions.

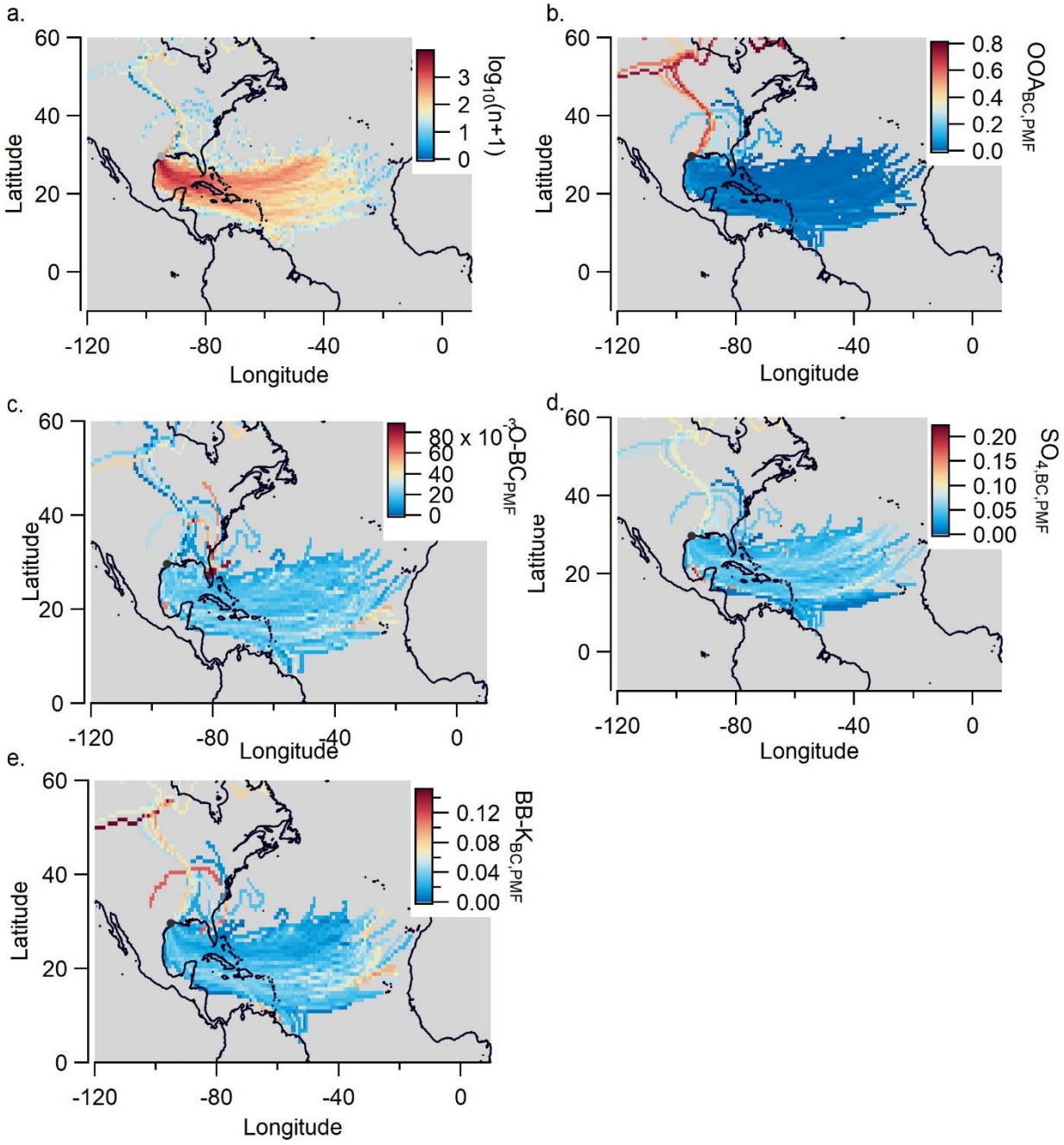

Figure S8: 14-day back trajectories from the La Porte sampling site originating every hour for the duration of the sampling period.
(a) Back-trajectory density (b-e) concentration weighted back trajectories for each PMF factor.

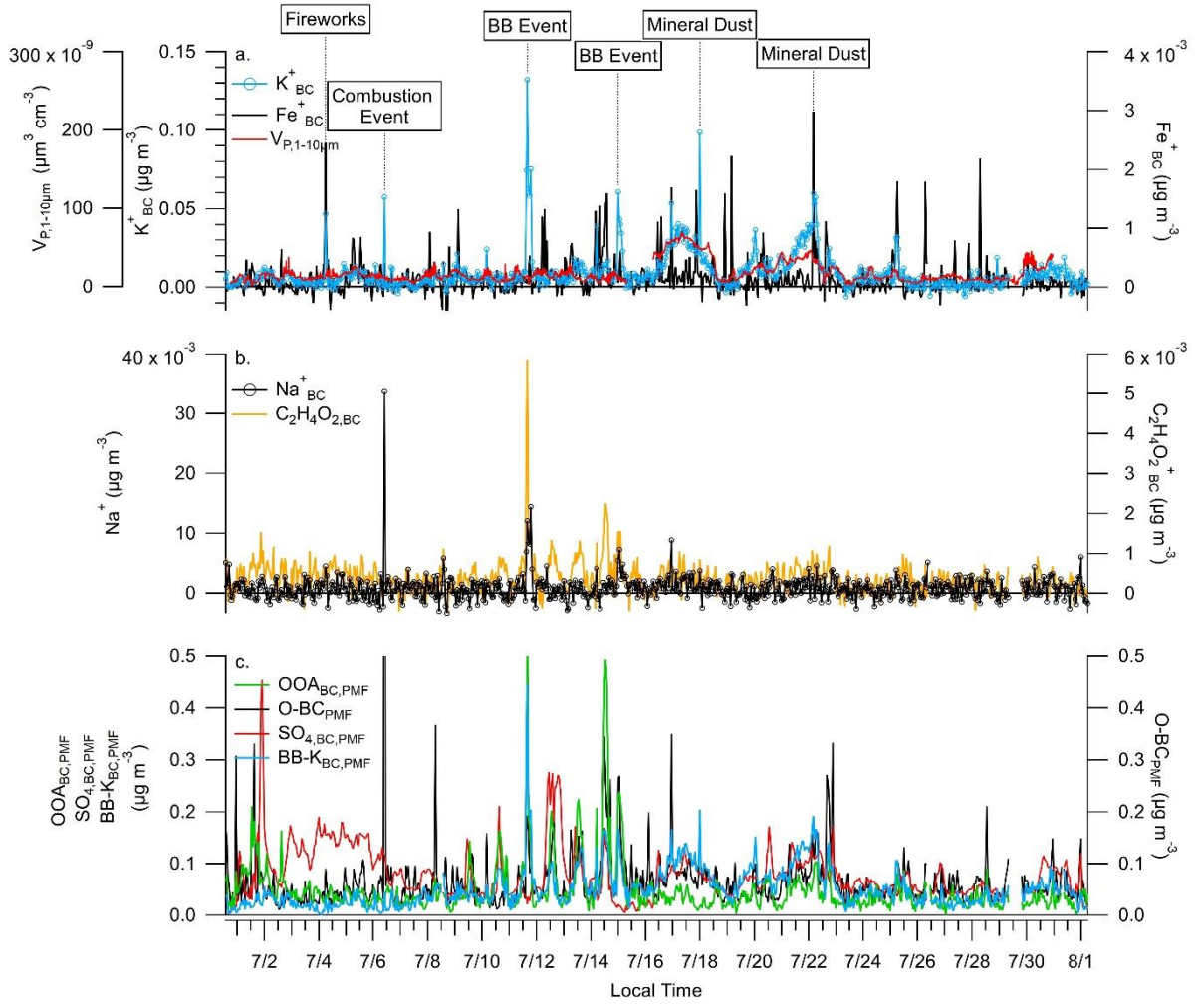

Figure S9: Time series comparison of (a) K^+ and Fe^+ measured by laser-only SP-AMS and aerosol volume between 1-10µm ($V_{1\text{-}10µm}$) measured by aerodynamic particle sizer. (b) Na^+ and $C_2H_4O_2^+$ measured by laser-only SP-AMS. (c) soot particle PMF factors. All species are averaged to one hour time resolution.

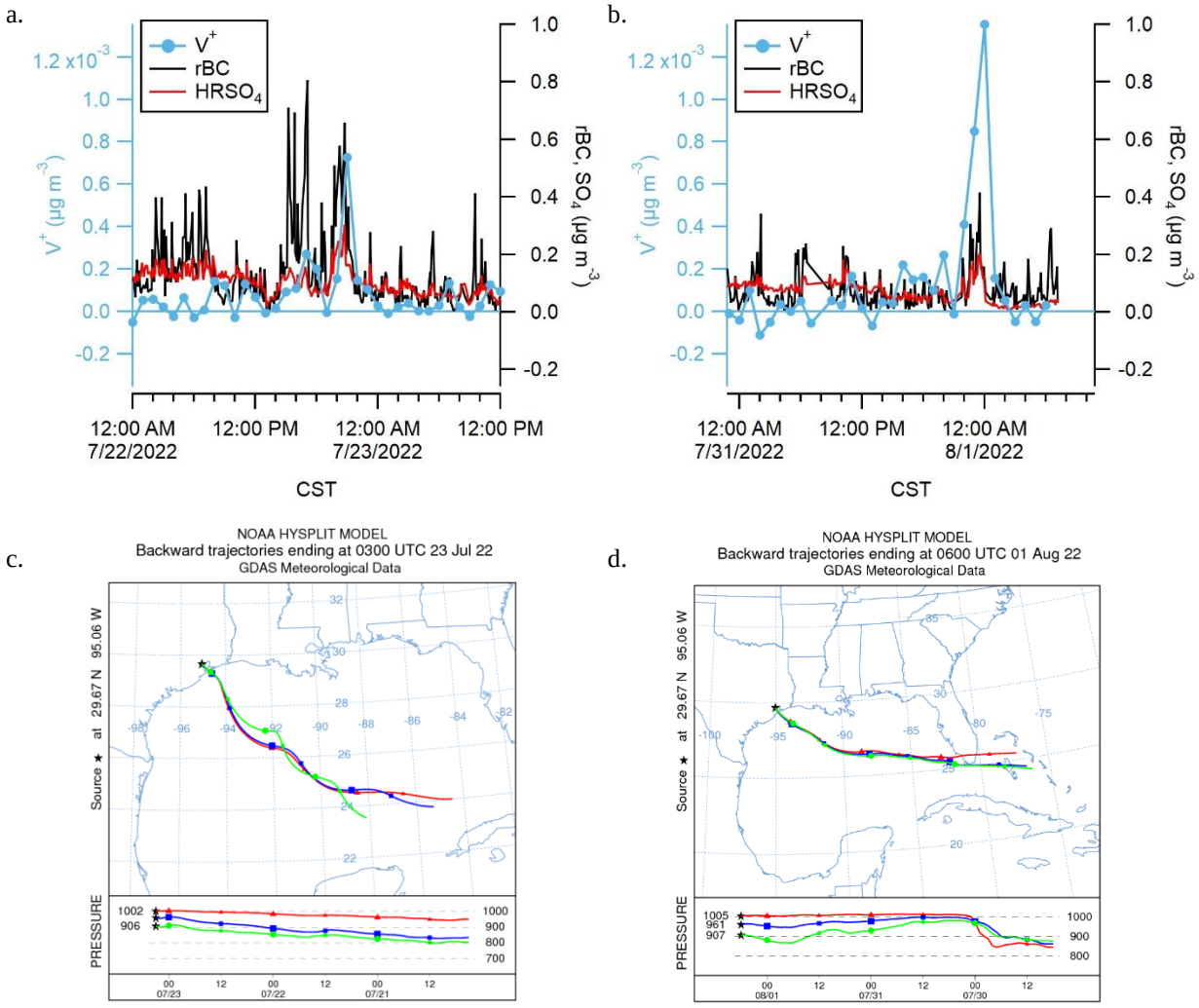

180 **Figure S10: (a, b) Time series of vanadium events on Jul 22 and Jul 31-Aug 1. Vanadium is presented in nitrate equivalent concentration and is averaged to one hour. (c, d) Hysplit back trajectory originating at the sampling site at the time of peak V^+ concentration.**

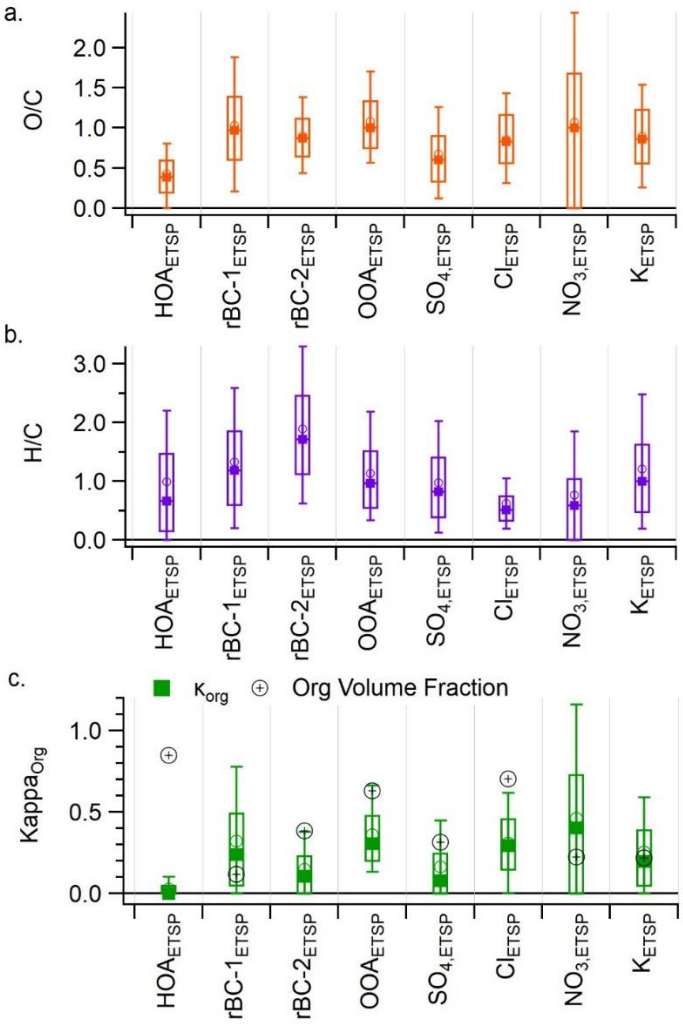

Figure S11: (a) OA O/C and (b) OA H/C ratio for single particle spectra, separated by particle class. (c) Kappa values calculated for the organic fraction of the single particle spectra, separated by particle class. Solid and open marker are the median and mean, box represents 25-75th percentile, whiskers represent 10-90th percentile. Cross symbols in (c) represent the average organic volume fraction of single particles.

Table S1: Single-particle signal threshold settings used during event trigger single particle (ETSP) measurements.

	Jun 30th – Jul 6th		Jul 6th – Aug 1st	
ROI	*m/z*	Trigger Level (ions)	*m/z*	Trigger Level (ions)
1	36	5	36	4
2	24	3	43	6
3	48	7.5	46-150	5.5

Table S2. Density and hygroscopicity parameters of pure compounds used in the calculation of κ.

Species	Density (g cm^{-3})	Hygroscopicity parameter (κ)
NH_4NO_3	1.72	0.67[1]
NH_4Cl	1.53	0.93[2]
$(NH_4)_2SO_4$	1.77	0.61[1]
K_2SO_4	2.66	0.69[2]
rBC	0.9	0
Organic	Variable[3]	Variable[4]

1. (Petters and Kreidenweis, 2007)
2. (Almeida et al., 2019)
3. (Kuwata et al., 2012)
4. (Duplissy et al., 2011)

Table S3: Number and percentage of particles in each ETSP class with no detectable rBC signal.

Class	Number of particles with no detectable rBC	Percent of particles with no detectable rBC
$HOA_{BC,ETSP}$	2949	77%
$BC\text{-}1_{ETSP}$	0	0%
$BC\text{-}2_{ETSP}$	157	10%
$OOA_{BC,ETSP}$	1351	48%
$SO_{4,BC,ETSP}$	2380	66%
$Cl_{BC,ETSP}$	279	38%
$NO_{3,BC,ETSP}$	236	96%
$K_{BC,ETSP}$	144	29%

210

References

Almeida, G. P., Bittencourt, A. T., Evangelista, M. S., Vieira-filho, M. S. and Estadual, U.: Characterization of aerosol chemical composition from urban pollution in Brazil and its possible impacts on the aerosol hygroscopicity and size distribution, Atmos. Environ., 202(March 2018), 149–159, doi:10.1016/j.atmosenv.2019.01.024, 2019.

Avery, A. M., Williams, L. R., Fortner, E. C., Robinson, W. A. and Onasch, T. B.: Particle detection using the dual-vaporizer configuration of the soot particle Aerosol Mass Spectrometer (SP-AMS), Aerosol Sci. Technol., 55(3), 254–267, doi:10.1080/02786826.2020.1844132, 2020.

Canagaratna, M. R., Jayne, J. T., Jimenez, J. L., Allan, J. D., Alfarra, M. R., Zhang, Q., Onasch, T. B., Drewnick, F., Coe, H., Middlebrook, A., Delia, A., Williams, L. R., Trimborn, A. M., Northway, M. J., DeCarlo, P. F., Kolb, C. E., Davidovits, P. and Worsnop, D. R.: Chemical and microphysical characterization of ambient aerosols with the aerodyne aerosol mass spectrometer, Mass Spectrom. Rev., 19(2), 173–181, doi:10.1002/mas.20115, 2007.

Canagaratna, M. R., Jimenez, J. L., Kroll, J. H., Chen, Q., Kessler, S. H., Massoli, P., Hildebrandt Ruiz, L., Fortner, E., Williams, L. R., Wilson, K. R., Surratt, J. D., Donahue, N. M., Jayne, J. T. and Worsnop, D. R.: Elemental ratio measurements of organic compounds using aerosol mass spectrometry: Characterization, improved calibration, and implications, Atmos. Chem. Phys., 15(1), doi:10.5194/acp-15-253-2015, 2015.

Cao, W., Martí-Rosselló, T., Li, J. and Lue, L.: Prediction of potassium compounds released from biomass during combustion, Appl. Energy, 250(May), 1696–1705, doi:10.1016/j.apenergy.2019.05.106, 2019.

Collier, S., Williams, L. R., Onasch, T. B., Cappa, C. D., Zhang, X., Russell, L. M., Chen, C. L., Sanchez, K. J., Worsnop, D. R. and Zhang, Q.: Influence of Emissions and Aqueous Processing on Particles Containing Black Carbon in a Polluted Urban Environment: Insights From a Soot Particle-Aerosol Mass Spectrometer, J. Geophys. Res. Atmos., 123(12), 6648–6666, doi:10.1002/2017JD027851, 2018.

DeCarlo, P. F., Kimmel, J. R., Trimborn, A., Northway, M. J., Jayne, J. T., Aiken, A. C., Gonin, M., Fuhrer, K., Horvath, T., Docherty, K. S., Worsnop, D. R. and Jimenez, J. L.: Field-deployable, high-resolution, time-of-flight aerosol mass spectrometer, Anal. Chem., doi:10.1021/ac061249n, 2006.

Draxler, R. R. and Hess, G. D.: An overview of the HYSPLIT_4 modelling system for trajectories, dispersion and deposition, Aust. Meteorol. Mag., 1998.

Duplissy, J., Decarlo, P. F., Dommen, J., Alfarra, M. R., Metzger, A., Barmpadimos, I. and Prevot, A. S. H.: Relating hygroscopicity and composition of organic aerosol particulate matter, Atmos. Chem. Phys., 1155–1165, doi:10.5194/acp-11-1155-2011, 2011.

Jayne, J. T., Leard, D. C., Zhang, X., Davidovits, P., Smith, K. A., Kolb, C. E. and Worsnop, D. R.: Development of an aerosol mass spectrometer for size and composition analysis of submicron particles, Aerosol Sci. Technol., doi:10.1080/027868200410840, 2000.

Kuwata, M., Zorn, S. R. and Martin, S. T.: Using elemental ratios to predict the density of organic material composed of carbon, hydrogen, and oxygen, Environ. Sci. Technol., 46(2), 787–794, doi:10.1021/es202525q, 2012.

Langridge, J. M., Richardson, M. S., Lack, D., Law, D. and Murphy, D. M.: Aircraft instrument for comprehensive characterization of aerosol optical properties, part i: Wavelength-dependent optical extinction and its relative humidity dependence measured using cavity ringdown spectroscopy, Aerosol Sci. Technol., 45(11), 1305–1318, doi:10.1080/02786826.2011.592745, 2011.

Onasch, T. B., Trimborn, A., Fortner, E. C., Jayne, J. T., Kok, G. L., Williams, L. R., Davidovits, P. and Worsnop, D. R.: Soot particle aerosol mass spectrometer: Development, validation, and initial application, Aerosol Sci. Technol., doi:10.1080/02786826.2012.663948, 2012.

Petit, J. E., Favez, O., Albinet, A. and Canonaco, F.: A user-friendly tool for comprehensive evaluation of the geographical origins of atmospheric pollution: Wind and trajectory analyses, Environ. Model. Softw., doi:10.1016/j.envsoft.2016.11.022, 2017.

Petters, M. D. and Kreidenweis, S. M.: A single parameter representation of hygroscopic growth and cloud condensation nucleus activity, Atmos. Chem. Phys., 13(2), 1081–1091, doi:10.5194/acp-13-1081-2013, 2007.

Pratt, K. A., Murphy, S. M., Subramanian, R., Demott, P. J., Kok, G. L., Campos, T., Rogers, D. C., Prenni, A. J., Heymsfield, A. J., Seinfeld, J. H. and Prather, K. A.: Flight-based chemical characterization of biomass burning aerosols within two prescribed burn smoke plumes, Atmos. Chem. Phys., 11(24), 12549–12565, doi:10.5194/acp-11-12549-2011, 2011.

Ulbrich, I. M., Canagaratna, M. R., Zhang, Q., Worsnop, D. R. and Jimenez, J. L.: Interpretation of organic components from Positive Matrix Factorization of aerosol mass spectrometric data, Atmos. Chem. Phys., doi:10.5194/acp-9-2891-2009, 2009.

Willis, M. D., Lee, A. K. Y., Onasch, T. B., Fortner, E. C., Williams, L. R., Lambe, A. T., Worsnop, D. R. and Abbatt, J. P. D.: Collection efficiency of the soot-particle aerosol mass spectrometer (SP-AMS) for internally mixed particulate black carbon, Atmos. Meas. Tech., doi:10.5194/amt-7-4507-2014, 2014.

Zauscher, M. D., Wang, Y., Moore, M. J. K., Gaston, C. J. and Prather, K. A.: Air quality impact and physicochemical aging of biomass burning aerosols during the 2007 San Diego wildfires, Environ. Sci. Technol., 47(14), 7633–7643, doi:10.1021/es4004137, 2013.

Zhang, Q., Jimenez, J. L., Canagaratna, M. R., Ulbrich, I. M., Ng, N. L., Worsnop, D. R. and Sun, Y.: Understanding atmospheric organic aerosols via factor analysis of aerosol mass spectrometry: A review, Anal. Bioanal. Chem., doi:10.1007/s00216-011-5355-y, 2011.